Hydrogen motion in C14-type $HfCr_2H_x$: quasielastic neutron scattering and NMR studies

2005 J. Phys.: Condens. Matter 17 5011

(http://iopscience.iop.org/0953-8984/17/33/006)

INSTITUTE OF PHYSICS PUBLISHING JOURNAL OF PHYSICS: CONDENSED MATTER

J. Phys.: Condens. Matter **17** (2005) 5011–5025 doi:10.1088/0953-8984/17/33/006

Hydrogen motion in C14-type $HfCr_2H_x$: quasielastic neutron scattering and NMR studies

A V Skripov[1], A V Soloninin[1], A L Buzlukov[1], L S Voyevodina[1], J C Cook[2], T J Udovic[2] and R Hempelmann[3]

[1] Institute of Metal Physics, Urals Branch of the Academy of Sciences, Ekaterinburg 620219, Russia
[2] NIST Center for Neutron Research, National Institute of Standards and Technology, Gaithersburg, MD 20899-8562, USA
[3] Institut für Physikalische Chemie, Universität des Saarlandes, D-66041 Saarbrücken, Germany

Received 20 May 2005
Published 5 August 2005
Online at stacks.iop.org/JPhysCM/17/5011

Abstract

In order to study the mechanism and parameters of hydrogen diffusion in the hexagonal (C14-type) Laves phase $HfCr_2$, we have performed quasielastic neutron scattering (QENS) measurements in $HfCr_2H_{0.74}$ and nuclear magnetic resonance (NMR) measurements of the proton spin-lattice relaxation rate in $HfCr_2H_x (0.30 \leqslant x \leqslant 1.62)$ over the temperature range 11–424 K. It is found that the diffusive motion of hydrogen in this system can be described in terms of at least two jump processes: a fast localized H motion with the jump rate τ_l^{-1} and a slower process with the rate τ_d^{-1} associated with H jumps leading to long-range diffusion. In the interval 175–400 K, the temperature dependences of both τ_l^{-1} and τ_d^{-1} are reasonably described by an Arrhenius law. For $HfCr_2H_{0.74}$ the corresponding activation energies derived from the QENS data are 122 ± 7 meV for τ_l^{-1} and 148 ± 7 meV for τ_d^{-1}; the ratio τ_d/τ_l at room temperature is close to 16. The long-range hydrogen mobility is found to decrease with increasing H content.

1. Introduction

Hydrogen diffusion in Laves phase intermetallic compounds AB_2 shows a number of interesting features including high H mobility down to low temperatures, unusual isotope effects and a coexistence of two frequency scales of H jump motion [1]. For the cubic (C15-type) Laves phases, the microscopic picture of H motion and the systematics of the two frequency scales of H motion are well understood [1–4]. In particular, in most of the studied cubic Laves phases where H atoms occupy only tetrahedral interstitial sites of g type (A_2B_2), the faster jump process corresponds to the localized H motion within the hexagons formed by g sites, and the slower process is associated with H jumps from one g-site hexagon to another. The difference between the characteristic frequencies of these jump processes is believed to result from the difference

Table 1. The lattice parameters of the hexagonal $HfCr_2H_x$ samples at room temperature.

Sample	a (Å)	c (Å)
$HfCr_2H_{0.30}$	5.096	8.310
$HfCr_2H_{0.60}$	5.110	8.381
$HfCr_2H_{0.74}$	5.114	8.413
$HfCr_2H_{0.87}$	5.128	8.420
$HfCr_2H_{1.62}$	5.206	8.539

between the g–g distances r_1 (within the hexagon) and r_2 (between the nearest hexagons). In contrast to the cubic Laves phases, the information on hydrogen diffusion in the hexagonal (C14-type) Laves phases is still fragmentary. The mobility of hydrogen has been studied in the C14-type $Ti_{1.2}Mn_{1.8}H_3$ [5], $TiCr_{1.9}H_x$ [6] and $ZrCr_2H_x$ [7–10]. Nuclear magnetic resonance (NMR) measurements of the proton spin-lattice relaxation rate [8] as well as the pulsed-field-gradient NMR measurements of the hydrogen diffusivity in C14-type $ZrCr_2H_{0.4}$ [9] have shown that the mobility of H atoms in this system is very high. At $T = 200$ K the measured hydrogen diffusion coefficient in $ZrCr_2H_{0.4}$ is about 2.3×10^{-8} cm^2 s^{-1} [9]. Quasielastic neutron scattering (QENS) experiments on C14-type $Ti_{1.2}Mn_{1.8}H_3$ [5] and $ZrCr_2H_{0.5}$ [10] also suggest a coexistence of at least two H jump processes with different characteristic rates. The aim of the present work is to study the microscopic picture and the parameters of H jump motion in C14-type $HfCr_2H_x$ using QENS and NMR measurements.

The intermetallic compound $HfCr_2$ is known to absorb considerable amounts of hydrogen forming solid solutions $HfCr_2H_x$ [11]. For hydrogen absorption at room temperature, the maximum value of x is about 1.6. Using hydrogen absorption at 193 K, it is possible to prepare $HfCr_2H_x$ samples with $x > 2$; however, these samples tend to decompose into two phases with different H concentrations [11]. The phase diagram of the $HfCr_2$–H system has not been studied so far. However, on the basis of the results for the isoelectronic $ZrCr_2$–H(D) system [12, 13] and the limited neutron diffraction data for $HfCr_2D_x$ [14], one may expect that in $HfCr_2H_x$ samples with $x > 0.6$ there is a low-temperature ($T < 200$ K) ordering of hydrogen. In the present work we report the results of our NMR measurements of the proton spin-lattice relaxation rate for $HfCr_2H_x$ ($0.30 \leqslant x \leqslant 1.62$), as well as QENS measurements for $HfCr_2H_{0.74}$. The QENS experiments are used to clarify the microscopic picture of H motion in $HfCr_2H_x$, and the NMR results allow us to trace the changes in the hydrogen jump rates due to the changes in the hydrogen concentration.

2. Experimental details

The $HfCr_2$ compound was prepared by arc melting high-purity Hf and Cr in a helium atmosphere. The resulting single-phase intermetallic was found to have the hexagonal C14-type structure with the lattice parameters $a = 5.067$ Å and $c = 8.259$ Å. Small pieces of $HfCr_2$ were charged with hydrogen in a Sieverts-type vacuum system. After annealing the sample in vacuum at 750 °C for 1 h, the calculated amounts of H_2 gas were admitted to the system at this temperature, typical hydrogen pressures being 0.3–0.5 bar. The samples were then slowly (for about 9 h) cooled down to room temperature in a hydrogen atmosphere, and the amounts of absorbed hydrogen were determined from the pressure drop in the calibrated volume of the system. According to x-ray diffraction analysis, all the hydrided samples are single-phase solid solutions with the C14-type host lattice; the compositions and the lattice parameters of the studied samples are listed in table 1.

QENS measurements for $HfCr_2H_{0.74}$ were performed on the Fermi-chopper time-of-flight spectrometer FCS (NIST Center for Neutron Research, Gaithersburg, Maryland) and on the high-resolution backscattering spectrometer IN10 (Institute Laue–Langevin (ILL), Grenoble). These two spectrometers complement each other with respect to the resolution and the accessible range of energy transfer, enabling one to probe H motion in the range of jump rates 10^8–10^{12} s^{-1}. In our experiments the incident neutron wavelengths were 6.0 Å (FCS) and 6.27 Å (IN10), the ranges of energy transfer $\hbar\omega$ studied were ± 700 μeV (FCS) and ± 14 μeV (IN10), and the energy resolution FWHMs were 65 μeV (FCS) and 1.0 μeV (IN10). The ranges of elastic momentum transfer $\hbar Q$ studied corresponded to Q-ranges of 0.34–1.92 $Å^{-1}$ (FCS) and 0.50–1.96 $Å^{-1}$ (IN10). For measurements on FCS, the powdered $HfCr_2H_{0.74}$ sample was placed into a hollow-cylinder Al container, and for measurements on IN10 it was placed into a flat Al container oriented nearly perpendicular to the incident beam. In both cases, the sample thickness was 0.3 mm. QENS spectra were recorded at $T = 40$, 270, 300, 330, 370 and 400 K (FCS) and at $T = 11$, 175, 269 and 298 K (IN10). The scattering angles corresponding to the Bragg reflections were excluded from the analysis (FCS) or shielded by cadmium (IN10). The raw experimental data were corrected for absorption and self-shielding using the standard NIST or ILL programs. For both spectrometers, the instrumental resolution functions were determined from the measured QENS spectra of $HfCr_2H_{0.74}$ at low temperatures (40 K for FCS and 11 K for IN10). The background spectra were measured for the empty sample containers in the same experimental geometry as for $HfCr_2H_{0.74}$.

NMR measurements of the proton spin-lattice relaxation rates R_1 were performed using a modernized Bruker SXP pulse spectrometer in the temperature range 11–424 K. The spin-lattice relaxation rates were measured by the saturation–recovery method at the resonance frequencies $\omega_0/2\pi$ in the range 13–90 MHz. In all cases the recovery of the nuclear magnetization could be fitted with a single exponential function.

3. Results and discussion

3.1. Quasielastic neutron scattering spectra

QENS spectra for $HfCr_2H_{0.74}$ measured on FCS at $T = 270$, 300 and 330 K can be satisfactorily described by a sum of two components: an 'elastic' line represented by the spectrometer resolution function $R(Q, \omega)$ and a resolution-broadened Lorentzian 'quasielastic' line. The relative intensity of the 'quasielastic' component is found to increase with increasing Q, its half-width being nearly Q-independent. These features are typical of the case of spatially restricted (localized) motion [15, 16]. However, at higher temperatures (370 and 400 K) the description in terms of a sum of an elastic line and a single Lorentzian quasielastic component leads to systematic deviations of the model QENS spectra from the experimental ones. For these temperatures, we have to add the second Lorentzian quasielastic component, so the experimental scattering function $S_{\mathrm{exp}}(Q, \omega)$ is fitted with the model incoherent scattering function,

$$S_{\mathrm{inc}}(Q, \omega) = A_0(Q)\delta(\omega) + A_1(Q)L(\omega, \Gamma_1) + A_2(Q)L(\omega, \Gamma_2) \tag{1}$$

convoluted with $R(Q, \omega)$. Here $\delta(\omega)$ is the elastic δ-function, $L(\omega, \Gamma)$ is the Lorentzian function with the half-width Γ and $A_0 + A_1 + A_2 = 1$. As an example of the data, figure 1 shows the QENS spectrum of $HfCr_2H_{0.74}$ recorded at 400 K for $Q = 1.81$ $Å^{-1}$. At the first stage of the analysis, we have used the model function (1) with all the amplitudes (A_0, A_1, A_2) and the half-widths (Γ_1, Γ_2) being independent fit parameters. The intensity of the broad quasielastic component, $A_2(Q)$, is found to increase with increasing Q, and its half-width Γ_2

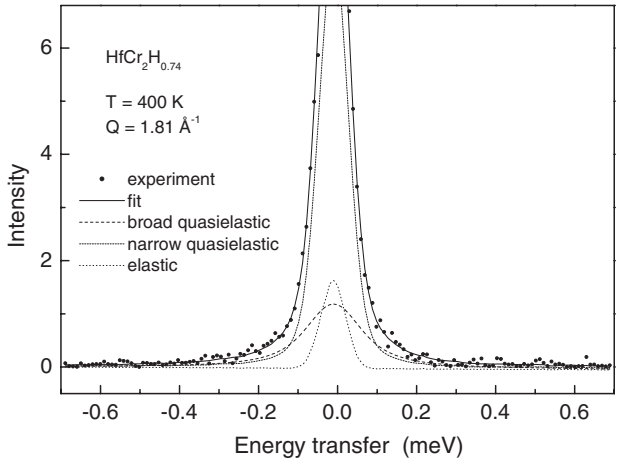

Figure 1. The QENS spectrum for $HfCr_2H_{0.74}$ measured on FCS at $T = 400$ K and $Q = 1.81$ Å^{-1}. The full curve shows the fit of the three-component model (equation (1)) to the data. The dotted line represents the elastic component (the spectrometer resolution function), and the broken curves show two Lorentzian quasielastic components.

appears to be nearly Q-independent. Since these features are typical of the spatially confined motion [15, 16], the broad quasielastic component can be attributed to the fast localized H motion with the jump rate τ_l^{-1}. In this case, the value of Γ_2 should be proportional to τ_l^{-1}, while the Q-dependence of A_2 should be related to the geometry of this motion. The half-width of the narrow quasielastic component, Γ_1, is found to increase with increasing Q, reaching a saturation in the Q-range 1.5–1.9 Å^{-1}. Furthermore, the value of Γ_1 increases strongly with increasing temperature. These features suggest that the narrow quasielastic component originates from a jump process leading to long-range H diffusion. The intensity of the elastic component, A_0, is found to be small (about 10% of the total scattered intensity), being nearly Q- and T-independent. This component can be attributed to the residual elastic contribution resulting mainly from the scattering by host–metal nuclei.

Since A_0 and Γ_2 appear to be nearly Q-independent, at the next stage of the analysis these parameters have been fixed (being equal to their average values at a given temperature). Thus, only A_1 and Γ_1 remain to be independent fit parameters, the value of A_2 being determined as $1 - A_0 - A_1$. In this case, the fitting procedure becomes quite stable. The solid curve in figure 1 shows the fit of the three-component model (equation (1)) to the data, and the broken curves represent contributions of the different components.

It is natural to assume that at lower temperatures (270–330 K) the value of Γ_1 is much smaller than the instrumental resolution half-width, so the narrow quasielastic component is not resolved and it contributes to the 'elastic' line intensity. In this temperature range, the time-of-flight QENS spectra have been analysed on the basis of equation (1) without the second term on the right-hand side. The fit parameters are A_0 and Γ_2, the value of A_0 being Q-dependent in this case.

QENS spectra for $HfCr_2H_{0.74}$ measured on the backscattering spectrometer IN10 at $T = 175$ K show the same qualitative features as those measured on FCS in the range 270–330 K. They can be satisfactorily described by a sum of the 'elastic' line and the single Lorentzian 'quasielastic' line with Q-dependent relative intensity and nearly Q-independent half-width. This means that at 175 K the long-range H diffusion is too slow to be resolved by

IN10, so only the faster localized H motion is observable. The backscattering QENS spectra at 175 K have been analysed on the basis of equation (1) without the second term on the right-hand side.

At $T = 269$ and 298 K the QENS spectra measured on IN10 can also be represented by a sum of the 'elastic' line and the single Lorentzian 'quasielastic' line. However, in this temperature range the relative intensity of the 'quasielastic' component is large and nearly Q-independent, while its half-width increases with increasing Q, reaching a saturation in the Q-range 1.5–1.9 Å^{-1}. These features are typical of a jump process leading to long-range H diffusion. The situation resembles that for the time-of-flight QENS spectra at $T = 370$ and 400 K; however, the broader 'quasielastic' component does not manifest itself in the backscattering QENS spectra. This means that at $T = 269$ and 298 K the jump rate of the localized H motion becomes much higher than the frequency 'window' of IN10, so the localized motion contributes only to the flat background in the spectra. The backscattering QENS spectra at 269 and 298 K have been analysed on the basis of equation (1) without the third term on the right-hand side.

3.2. Parameters of hydrogen motion in $HfCr_2H_{0.74}$ resulting from the QENS measurements

Figures 2 and 3 show the Q-dependences of the half-width Γ_1 of the narrow quasielastic line, as derived from the QENS spectra measured on FCS and IN10, respectively. For parametrization of these dependences, we have used the orientationally averaged Chudley–Elliott model [17]. The corresponding form of $\Gamma_1(Q)$ is

$$\Gamma_1(Q) = \frac{\hbar}{\tau_d}\left(1 - \frac{\sin QL}{QL}\right), \tag{2}$$

where τ_d is the mean time between two successive H jumps leading to long-range diffusion, and L is the effective jump length. The fits of equation (2) to the data are shown by the solid curves in figures 2 and 3. The temperature dependence of the jump rate τ_d^{-1} resulting from the Chudley–Elliott fits is presented in figure 4. As can be seen from this figure, the values of τ_d^{-1} derived from the measurements on FCS and IN10 are likely to originate from the same motional process described by an Arrhenius law

$$\tau_d^{-1} = \tau_{d0}^{-1} \exp(-E_a^d/k_B T), \tag{3}$$

where E_a^d is the activation energy for hydrogen diffusion. The lower solid line in figure 4 shows the global Arrhenius fit to the τ_d^{-1} data (including both the FCS and IN10 results); the corresponding fit parameters are $E_a^d = 148 \pm 7$ meV and $\tau_{d0}^{-1} = (1.2 \pm 0.3) \times 10^{12}$ s^{-1}.

The values of L resulting from the Chudley–Elliott fits tend to increase with increasing temperature; they change from 2.1 ± 0.1 Å at 269 K to 2.58 ± 0.16 Å at 400 K. It should be noted that the fitted values of the effective jump length are always considerably longer than the distances between the nearest-neighbour interstitial sites (1.1–1.2 Å) in the C14-type structure. This feature appears to be common for a number of Laves phase hydrides [1, 2, 4, 10, 18, 19]. It will be discussed in more detail below.

We now turn to a discussion of the parameters of the faster jump process associated with localized H motion. The geometry of the localized H motion can, in principle, be derived from the Q-dependence of the elastic incoherent structure factor (EISF) [15, 16]. For QENS spectra described by equation (1) (such as the spectra measured on FCS at $T = 370$ and 400 K), the 'resolution-limited' EISF is defined as $(A_0+A_1)/(A_0+A_1+A_2) = A_0+A_1$. Assuming that the purely elastic component of these QENS spectra originates from the host-metal contribution to the incoherent scattering function, we can conclude that the EISF for the hydrogen sublattice is determined by the ratio $A_1/(A_1+A_2)$. For QENS spectra described by equation (1) without

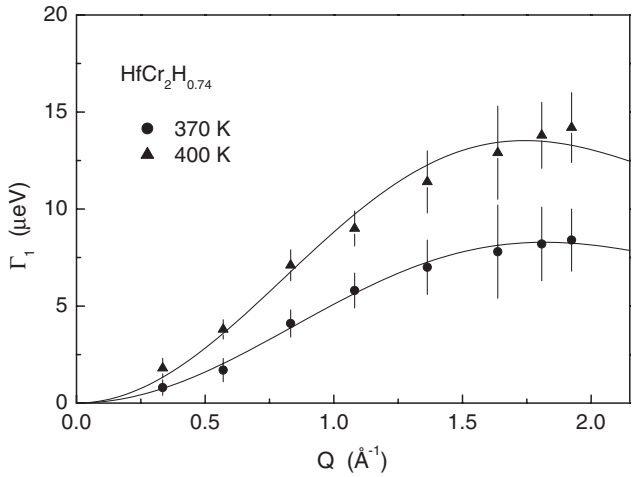

Figure 2. The half-width (HWHM) of the narrow Lorentzian QENS component for $HfCr_2H_{0.74}$ as a function of Q measured on FCS at $T = 370$ and 400 K. The full curves show the fits of the Chudley–Elliott model (equation (2)) to the data.

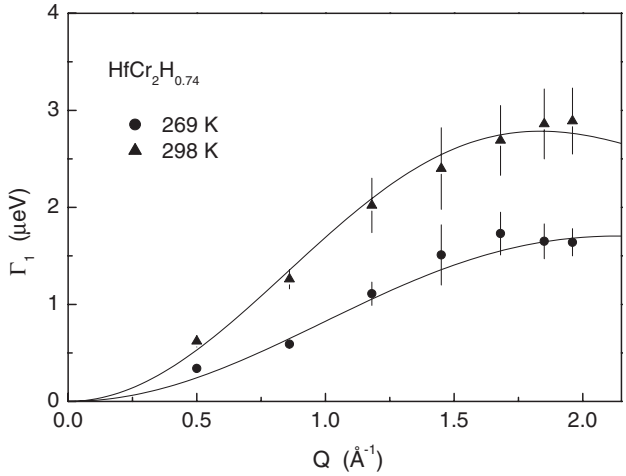

Figure 3. The half-width (HWHM) of the narrow Lorentzian QENS component for $HfCr_2H_{0.74}$ as a function of Q measured on IN10 at $T = 269$ and 298 K. The solid curves show the fits of the Chudley–Elliott model (equation (2)) to the data.

the second term (such as the spectra measured on FCS at $T = 270$, 300 and 330 K and the spectra measured on IN10 at $T = 175$ K), the EISF for the hydrogen sublattice is determined by the ratio $A_0/(A_0 + A_2)$, where A_0 should be corrected for the host-metal contribution. As an example of the data, figure 5 shows the Q-dependence of the EISF at $T = 300$ and 400 K. The observed Q-dependences of the EISF at other temperatures have similar shapes. As can be seen from figure 5, the measured EISF appears to be temperature dependent, decreasing with increasing T. This feature is common for all the studied Laves phase hydrides [1–4, 10]. In order to account for this feature, we have to assume that only a fraction p of the H atoms participates in the fast localized motion, and this fraction increases with temperature. The existence of 'static' H atoms may result from the H–H interaction leading to the formation of

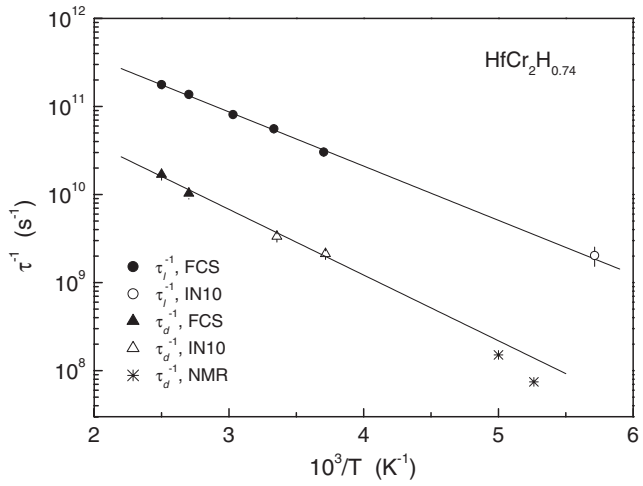

Figure 4. The hydrogen jump rates τ_l^{-1} and τ_d^{-1} in $HfCr_2H_{0.74}$ as functions of the inverse temperature. The jump rates are obtained from the QENS spectra measured on FCS (solid symbols) and IN10 (open symbols). The full lines show the global Arrhenius fits to the QENS data for τ_l^{-1} and τ_d^{-1}. The stars represent the H jump rates derived from the maxima of the proton spin-lattice relaxation rates at two resonance frequencies.

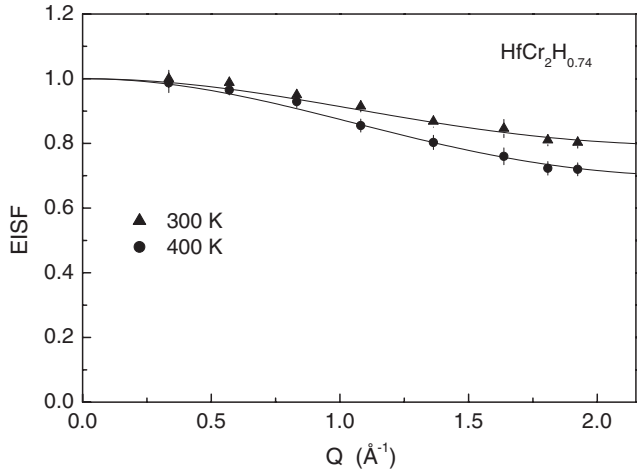

Figure 5. The elastic incoherent structure factor for $HfCr_2H_{0.74}$ as a function of Q measured on FCS at $T = 300$ and 400 K. The full curves show the fits of the six-site model (equation (4)) with the fixed $r = 1.16$ Å to the data.

some ordered atomic configurations at low temperatures. Such an explanation is supported by the observation of the long-range ordering of D in $HfCr_2D_{0.8}$ below 160 K [14].

In order to discuss the microscopic picture of H motion, we have to consider the spatial arrangement of the interstitial sites occupied by hydrogen. On the basis of the general trends of site occupancy in hydrides of intermetallics [12, 20] and the neutron diffraction data for $HfCr_2D_x$ [14], we may conclude that in the studied range of hydrogen concentrations, H atoms in $HfCr_2H_x$ occupy only the tetrahedral sites with $[Hf_2Cr_2]$ coordination. There are four inequivalent types of such sites in the C14-type lattice: h_1, h_2, k and l. The spatial

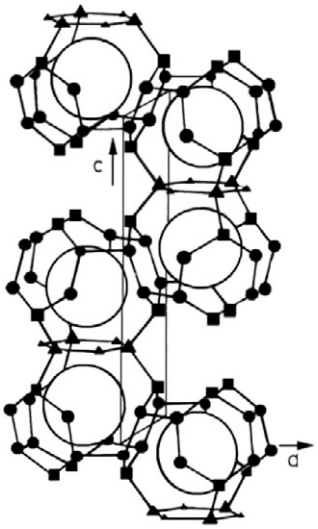

Figure 6. The spatial arrangement of interstitial [Hf_2Cr_2] sites in C14-type $HfCr_2$ (from [21]). Large triangles: h_1 sites; small triangles: h_2 sites; squares: k sites; solid circles: l sites; large open circles: Hf atoms.

arrangement of these sites is shown in figure 6. As in the case of the C15 structure, the sublattice of [Hf_2Cr_2] sites consists of hexagons; however, these hexagons are formed by inequivalent sites. Type I hexagons are in the basal plane; they are formed by alternating h_1 and h_2 sites. Type II hexagons are formed by two k and four l sites in the sequence k–l–l–k–l–l. In order to calculate the intersite distances, we have used the actual lattice parameters a and c of $HfCr_2H_{0.74}$ and the positional parameters of D atoms in h_1, h_2, k and l sites found for the related compound $ZrMn_2D_3$ [21]. The following distances between the nearest neighbours have been obtained:

h_1–h_2 (within type I hexagons): $r_3 = 1.15$ Å;
l–l (within type II hexagons): $r_4 = 1.11$ Å;
k–l (within type II hexagons): $r_5 = 1.18$ Å;
h_1–k (between type I and type II hexagons): $r_6 = 1.23$ Å;
l–l (between two type II hexagons): $r_7 = 1.24$ Å.

Since the distances between the nearest sites within the hexagons (r_3, r_4, r_5) are shorter than the distances between the nearest sites on different hexagons (r_6, r_7), we may expect that (similarly to the case of C15-type compounds [1–4]) the localized H motion in $HfCr_2H_{0.74}$ occurs within the hexagons. For the model of jumps between six equidistant sites on a circle of radius r [15, 16], the Q-dependence of the EISF is given by

$$\mathrm{EISF} = 1 - p + \frac{p}{6}[1 + 2j_0(Qr) + 2j_0(Qr\sqrt{3}) + j_0(2Qr)], \tag{4}$$

where $j_0(x)$ is the spherical Bessel function of zeroth order. Neglecting the small difference between type I and type II hexagons, we may try to use equation (4) to fit the experimental Q-dependence of the EISF. Such a fit at $T = 400$ K (corresponding to the strongest variation of the EISF) yields $p = 0.37 \pm 0.05$, $r = 1.08 \pm 0.11$ Å. The fitted value of r is close to the weighted average of r_3, r_4 and r_5, $\overline{r} = 1.16$ Å. By fixing the value of r to 1.16 Å, we have found reasonable fits of the six-site model (equation (4)) to the data at all the temperatures studied

with p as the only fit parameter. The results of these fits are shown as full curves in figure 5. The fitted values of p increase with increasing temperature, changing from 0.21 ± 0.01 at 270 K to 0.34 ± 0.01 at 400 K.

The half-width Γ_2 of the broader quasielastic line is proportional to the hydrogen jump rate τ_l^{-1} of the localized motion. The exact relation between Γ_2 and τ_l^{-1} depends on the geometry of the localized motion. For the six-site localized motion, $\Gamma_2 \approx 0.6\hbar\tau_l^{-1}$ [15] at $Qr < 1.5$ (which approximately corresponds to our experimental Q-range). The values of τ_l^{-1} derived from the half-widths of the broader quasielastic line as $\tau_l^{-1} = \Gamma_2/0.6\hbar$ are shown in figure 4. As can be seen from this figure, the values of τ_l^{-1} obtained from the measurements on FCS and IN10 are likely to originate from the same motional process described by an Arrhenius law

$$\tau_l^{-1} = \tau_{l0}^{-1} \exp(-E_a^l/k_B T), \tag{5}$$

where E_a^l is the activation energy for the localized H motion. The upper full line in figure 4 represents the global Arrhenius fit to the τ_l^{-1} data (including both the FCS and IN10 results); the corresponding fit parameters are $E_a^l = 122 \pm 7$ meV and $\tau_{l0}^{-1} = (6.1 \pm 1.5) \times 10^{12}\ s^{-1}$. The activation energy for the localized H motion appears to be lower than that for the long-range H diffusion. At room temperature the jump rate τ_l^{-1} is a factor of 16 higher than τ_d^{-1}. The ratio τ_d/τ_l at 300 K for $HfCr_2H_{0.74}$ is close to that found for the related C15-type system $ZrCr_2H_x$ (τ_d/τ_l (300 K) $\approx$ 20) [1]. However, this ratio is two orders of magnitude smaller than that for the C15-type TaV_2H_x [1].

It should be noted that a more rigorous treatment of the six-site localized motion with the jump rate τ_l^{-1} leads to a coexistence of three broad Lorentzian components with the half-widths of $0.5\hbar\tau_l^{-1}$, $1.5\hbar\tau_l^{-1}$ and $2\hbar\tau_l^{-1}$ and the Q-dependent amplitudes [15, 16]. However, as has been shown previously [2, 10, 22], on the basis of the experimental data at $Qr < 1.5$ it is practically impossible to distinguish between such a three-component quasielastic line and a single Lorentzian with a Q-independent width $\Gamma_2 \approx 0.6\hbar\tau_l^{-1}$. Since, in our case, part of the observed QENS spectra have an additional complicating feature (the resolved narrow quasielastic component with the half-width Γ_1), we have used the simplified approach to derive the values of τ_l^{-1}. The Q-dependence of the EISF is described by equation (4) in both approaches.

We now return to a discussion of the values of L derived from the Chudley–Elliott analysis of $\Gamma_1(Q)$. As mentioned above, these values appear to be considerably larger than the distances between the nearest-neighbour interstitial sites (r_3–r_7). This feature can be naturally accounted for in terms of the model of H motion with two frequency scales: the rate τ_l^{-1} of jumps within the hexagons and the rate τ_d^{-1} of jumps between the hexagons, $\tau_d^{-1} \ll \tau_l^{-1}$. As explained in [2, 10], this model implies that τ_d is the mean residence time of a hydrogen atom *at a hexagon* (not at an interstitial site, as usually). Since a hydrogen atom may enter a hexagon through one site and leave it from the other site, the total displacement for the time τ_d is the distance between the nearest sites on different hexagons plus the additional displacement between the initial and final positions of a hydrogen atom at the hexagon. The half-width Γ_1 is determined by the slower time scale τ_d^{-1}; therefore the apparent jump length L derived from the Q-dependence of Γ_1 is larger than the distances between the nearest-neighbour interstitial sites. The observed growth of L with increasing temperature may be related [10] to the increasing fraction p of H atoms participating in the fast localized motion.

3.3. Proton spin-lattice relaxation rates

The measured proton spin-lattice relaxation rate R_1 in metal–hydrogen systems usually results from the sum of contributions due to conduction electrons (R_{1e}) and the internuclear dipole–

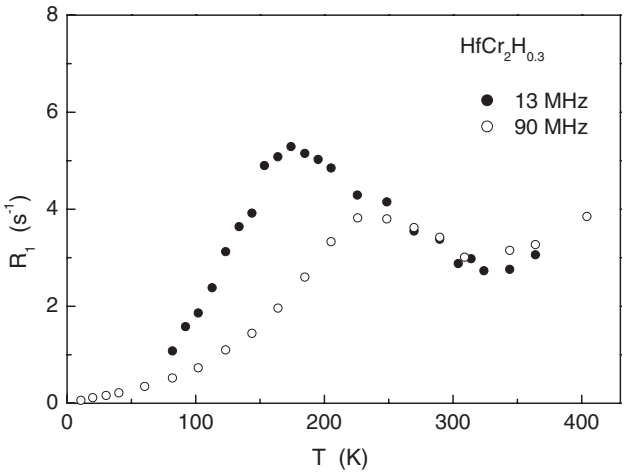

Figure 7. The temperature dependence of the proton spin-lattice relaxation rate for $HfCr_2H_{0.30}$ measured at 13 and 90 MHz.

dipole interaction modulated by H motion (R_{1d}) [23]:

$$R_1 = R_{1e} + R_{1d}. \tag{6}$$

At low temperatures, the motional contribution is negligible, so the relaxation rate is determined by the frequency-independent electronic (Korringa) contribution which is typically proportional to the temperature, $R_{1e} = C_e T$. The frequency-dependent motional contribution R_{1d} becomes more important in the temperature range where the hydrogen jump rate τ^{-1} is between 10^6 and 10^{10} s^{-1}. The temperature dependence of R_{1d} is expected to have a characteristic peak at the temperature at which $\omega_0\tau \approx 1$.

For all the samples studied, the measured proton spin-lattice relaxation rates exhibit a linear temperature dependence at low T and a frequency-dependent peak in the range 160–230 K. As examples of the experimental data, figures 7–9 show the temperature dependences of R_1 in $HfCr_2H_{0.30}$, $HfCr_2H_{0.74}$ and $HfCr_2H_{1.62}$ measured at several resonance frequencies. The values of C_e resulting from the $R_1(T)$ data at $\omega_0/2\pi = 90$ MHz and $T < 60$ K are listed in table 2. It can be seen that the value of C_e characterizing the strength of the electronic contribution increases significantly with increasing H content. In transition-metal–hydrogen systems, C_e is usually dominated by the spin contribution of d electrons [23] proportional to the square of the density of d-electron states at the Fermi level, $N_d^2(E_F)$. Therefore our low-T experimental data suggest that in $HfCr_2H_x$ the value of $N_d(E_F)$ increases with increasing x. This is consistent with the results of the magnetic susceptibility measurements for $HfCr_2H_x(D_x)$ [24]. A similar behaviour of $N_d(E_F)$ as a function of x has also been reported for the isoelectronic systems $TiCr_{1.8}H_x$ [25] and $ZrCr_2H_x$ [8, 26]. An increase in $N_d(E_F)$ with increasing H content may be expected if for the H-free compound the Fermi level lies below a peak in the density of electron states.

Above room temperature the proton relaxation rates for $HfCr_2H_x$ should also be dominated by the electronic contribution. In fact, at $T > 330$ K the measured relaxation rates increase with increasing temperature (figures 7–9), whereas the motional contribution R_{1d} is expected to decrease in this range. However, for all the samples studied, the values of R_1 at $T > 330$ K are considerably higher than those obtained from the linear extrapolation of the low-temperature $R_{1e}(T)$ results. A similar feature has been found for the isoelectronic system $ZrCr_2H_x$ [26].

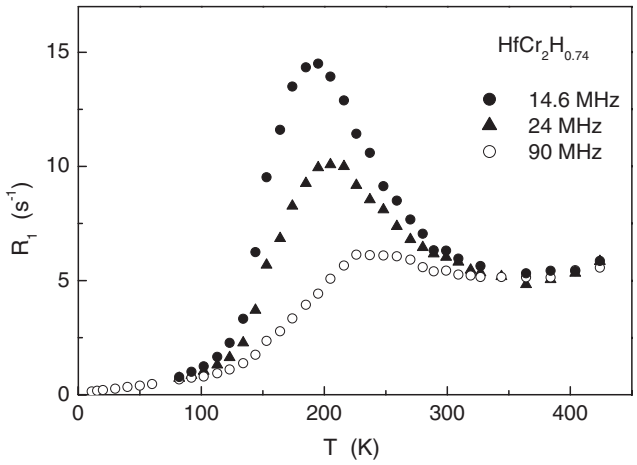

Figure 8. The temperature dependence of the proton spin-lattice relaxation rate for $HfCr_2H_{0.74}$ measured at 14.6, 24 and 90 MHz.

Table 2. The parameters resulting from the analysis of the proton spin-lattice relaxation rates in $HfCr_2H_x$. The values of C_e and B characterize the electronic contribution to R_1 (equation (7)). The maximum motional contributions to the relaxation rate, $(R_{1d})_{max}$, and the temperatures of this maximum, T_{max}, are obtained from the data at the lowest resonance frequency of our measurements (14.6 MHz for $HfCr_2H_{0.74}$ and 13 MHz for the other samples). The average activation energies for H diffusion, $\overline{E}_a^d$, and the pre-exponential factors, τ_{d0}^{-1}, result from the analysis based on the BPP model with a Gaussian distribution of activation energies (equations (3), (8) and (9)).

Sample	C_e (s^{-1} K^{-1})	B (s^{-1} K^{-3})	$(R_{1d})_{max}$ (s^{-1})	T_{max} (K)	$\overline{E}_a^d$ (meV)	τ_{d0}^{-1} (s^{-1})
$HfCr_2H_{0.30}$	5.38×10^{-3}	2.24×10^{-8}	4.24	174	138	1.1×10^{12}
$HfCr_2H_{0.60}$	6.36×10^{-3}	3.17×10^{-8}	9.11	179	147	1.2×10^{12}
$HfCr_2H_{0.74}$	6.94×10^{-3}	4.24×10^{-8}	12.8	190	141	4.3×10^{11}
$HfCr_2H_{0.87}$	8.24×10^{-3}	8.27×10^{-8}	16.8	185	151	9.1×10^{11}
$HfCr_2H_{1.62}$	2.07×10^{-2}	1.04×10^{-7}	40.3	201	177	1.8×10^{12}

This feature may originate from nonlinear contributions to $R_{1e}(T)$ at high temperatures [27] or from a phase transition accompanied by a change in $N_d(E_F)$ at intermediate temperatures. In order to evaluate the motional contribution $R_{1d}(T)$, we assume here that the observed behaviour of $R_{1e}(T)$ is governed by nonlinear terms. These terms may appear due to a rapid variation of $N_d(E)$ near the Fermi level; in the first approximation the electronic contribution to the relaxation rate is given by [27]

$$R_{1e} = C_e T + B T^3. \tag{7}$$

The values of B resulting from the fit of equation (7) to the relaxation rate data in both the low-temperature and the high-temperature regions are shown in table 2.

The motional contribution to the proton spin-lattice relaxation rate has been evaluated as $R_{1d} = R_1 - R_{1e}$ where R_{1e} is given by equation (7) with the parameters C_e and B listed in table 2. As examples of the results, figures 10 and 11 show the temperature dependences of R_{1d} for $HfCr_2H_{0.74}$ and $HfCr_2H_{1.62}$. Included in table 2 are the temperatures T_{max} of the R_{1d} maximum and the maximum values of R_{1d} for all the samples at the lowest resonance frequency of our measurements. The maximum values of R_{1d} for $HfCr_2H_x$ strongly increase with increasing x.

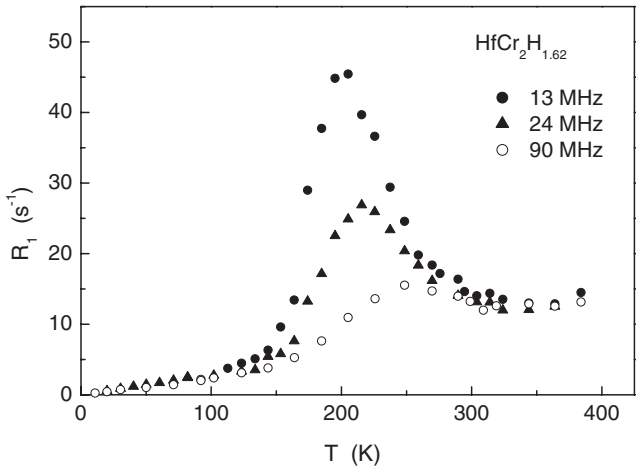

Figure 9. The temperature dependence of the proton spin-lattice relaxation rate for $HfCr_2H_{1.62}$ measured at 13, 24 and 90 MHz.

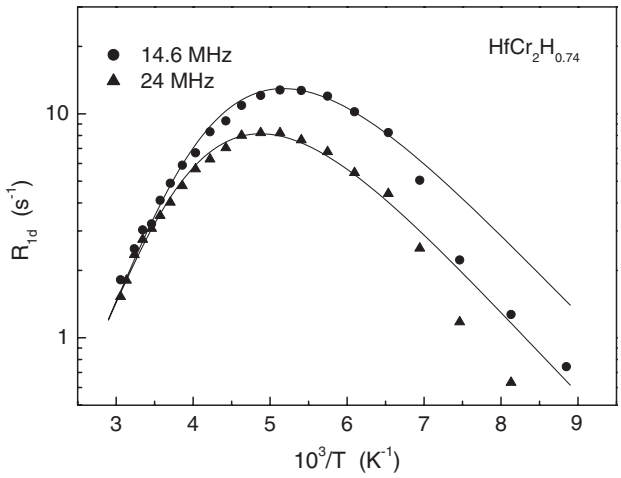

Figure 10. The motional contribution to the proton spin-lattice relaxation rate for $HfCr_2H_{0.74}$ as a function of the inverse temperature at 14.6 and 24 MHz. The full curves represent the fit of the BPP model with a Gaussian distribution of activation energies to the data at $T > 160$ K.

This feature is consistent with the dominant contribution of the H–H dipole–dipole interaction to R_{1d}. In fact, because of the low natural abundance of the host-metal isotopes with non-zero nuclear spins (^{177}Hf, ^{179}Hf and ^{53}Cr) and their small gyromagnetic ratios, we can neglect the contribution to R_{1d} arising from dipole–dipole interactions between protons and host-metal nuclei. As can be seen from table 2, the value of T_{max} for $HfCr_2H_x$ tends to increase with increasing x. This means that, for the motional process responsible for the R_{1d} maximum, the characteristic H jump rate decreases with increasing H content.

In order to identify the motional process responsible for the R_{1d} maximum, we have evaluated the hydrogen jump rates τ^{-1} corresponding to the R_{1d} maxima in $HfCr_2H_{0.74}$ at $\omega_0/2\pi = 14.6$ and 24 MHz and included these values in figure 4. The values of τ^{-1} at the relaxation rate maxima have been derived from the condition $\omega_0\tau = 1.23$ corresponding to

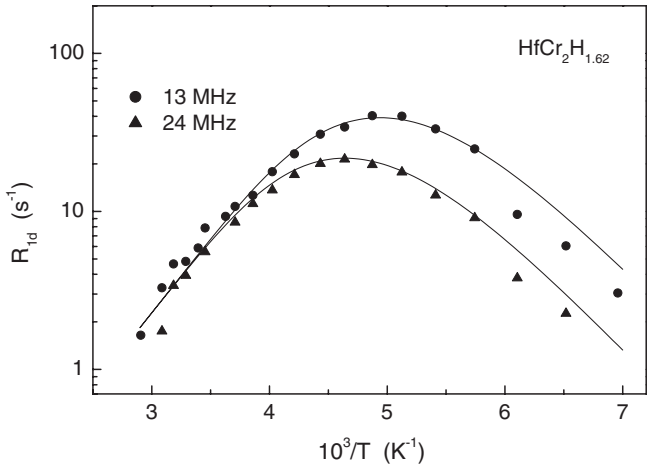

Figure 11. The motional contribution to the proton spin-lattice relaxation rate for $HfCr_2H_{1.62}$ as a function of the inverse temperature at 13 and 24 MHz. The full curves represent the fit of the BPP model with a Gaussian distribution of activation energies to the data at $T > 160$ K.

the Bloembergen–Purcell–Pound (BPP) model [28]. It can be seen from figure 4 that these values of τ^{-1} are close to the extrapolation of the Arrhenius plot of $\tau_d^{-1}(T)$ obtained from the QENS data for $HfCr_2H_{0.74}$. This suggests that the R_{1d} maximum originates from the slower jump process leading to long-range H diffusion, i.e. τ^{-1} should be identified with τ_d^{-1}. For cubic Laves phase hydrides having very large τ_d/τ_l ratios, the faster jump rate gives rise to an additional low-temperature peak of the proton spin-lattice relaxation rate [29, 30]. However, for other cubic Laves phase hydrides including $TiCr_2H_x$ [6], $ZrCr_2H_x$ [8, 26, 31], HfV_2H_x and ZrV_2H_x [32, 33] and $ZrMo_2H_x$ [34] the proton relaxation rate does not show any additional low-temperature peak. For these compounds the τ_d/τ_l ratios are not large enough to give rise to a well-resolved additional $R_{1d}(T)$ peak, so the faster H jump process contributes only to the low-temperature slope of the single-peak $R_{1d}(T)$ dependence. A similar situation corresponds to our R_1 results for the hexagonal $HfCr_2H_x$ system. In this case the observed behaviour of the proton spin-lattice relaxation rate near the $R_{1d}(T)$ maximum may be parametrized in terms of the BPP model with a Gaussian distribution of the activation energies E_a^d [26, 32]. Such a simplified description is expected to yield reasonable estimates of the parameters of the slower H jump process (τ_{d0}^{-1} and the average value of E_a^d); however, it cannot give any information on the faster H jump process.

For a single value of E_a^d, the motional contribution to the proton spin-lattice relaxation rate in terms of the BPP model can be written as

$$R_{1d}(E_a^d) = \frac{4M_2}{3\omega_0}\left[\frac{y}{4+y^2} + \frac{y}{1+y^2}\right], \tag{8}$$

where M_2 is the 'rigid-lattice' second moment of the proton NMR line, $y = \omega_0\tau_d$ and $\tau_d(T)$ is given by equation (3). In the presence of a distribution of E_a^d values, $G(E_a^d)$, the relaxation rate is given by

$$R_{1d} = \int R_{1d}(E_a^d)G(E_a^d)\,dE_a^d. \tag{9}$$

For a Gaussian shape of $G(E_a^d)$, the parameters of the model are M_2, τ_{d0}, the average activation energy $\overline{E}_a^d$ and the distribution width (dispersion) ΔE_a^d. We have found that for $HfCr_2H_x$

samples with $x > 0.6$, this model can reasonably describe the experimental data only at $T > 160$ K. The observed drop of R_{1d} below 160 K (or above $10^3/T \approx 6.3$ K^{-1}, see figures 10 and 11) cannot be accounted for in terms of the BPP model or more sophisticated models of the proton spin relaxation due to H diffusion (see, e.g., [35]). Such a drop may result from a hydrogen ordering that leads to a sharp decrease [33] in the H jump rate. The ordering of hydrogen in $HfCr_2H_x$ in this temperature range is consistent with the neutron diffraction data [14]. We look for a set of parameters giving the best fit to the R_{1d} at two resonance frequencies *simultaneously*. The results of such simultaneous fits to the data at $T > 160$ K are shown by full curves in figures 10 and 11. The parameters $\overline{E}_a^d$ and τ_{d0}^{-1} resulting from the fits for all the samples studied are presented in table 2. Note that for $HfCr_2H_{0.30}$ and $HfCr_2H_{0.60}$ we have not found any effects of H ordering on R_{1d}, so the fits for these samples have been made over broader temperature ranges ($T > 100$ K). The estimated uncertainty in the average activation energies is ± 8 meV. As can be seen from table 2, the value of $\overline{E}_a^d$ tends to increase with increasing H content. For $HfCr_2H_{0.74}$ the value of $\overline{E}_a^d$ derived from the NMR data is close to the value of E_a^d (148 ± 7 meV) found from the QENS results. For the samples with $x > 0.6$, the distribution widths ΔE_a^d resulting from our fits are in the range 16–25 meV. These values are considerably lower than the average activation energies. This means that the behaviour of R_{1d} at $T > 160$ K for $HfCr_2H_x$ with $x > 0.6$ can be reasonably accounted for even without any distribution of the activation energies. For $HfCr_2H_{0.30}$ and $HfCr_2H_{0.60}$ the fitted values of ΔE_a^d are larger (43 and 32 meV, respectively). It should be noted, however, that as in the case of C15-type $ZrCr_2H_x$ [26, 31], the fitted values of ΔE_a^d may depend on the contribution of the faster jump process to the low-temperature slope of $R_{1d}(T)$; therefore, the model values of ΔE_a^d may have no clear physical meaning. In contrast, the value of $\overline{E}_a^d$ (which is determined by the high-temperature slope of $R_{1d}(T)$) must be a real physical parameter describing the temperature dependence of the hydrogen jump rate τ_d^{-1}.

4. Conclusions

The analysis of our quasielastic neutron scattering data for C14-type $HfCr_2H_{0.74}$ has shown that the diffusive motion of hydrogen in this system can be described in terms of at least two jump processes with different frequency scales. The faster process with the jump rate τ_l^{-1} corresponds to localized H motion, and the slower process with the jump rate τ_d^{-1} is associated with H jumps leading to long-range diffusion. The ratio of the jump rates for these two processes, τ_d/τ_l, at room temperature is found to be close to 16. For both jump processes, the temperature dependence of the hydrogen jump rate is reasonably described by an Arrhenius law over the temperature ranges studied; the corresponding activation energies are 122 ± 7 meV for τ_l^{-1} (in the range 175–400 K) and 148 ± 7 meV for τ_d^{-1} (in the range 269–400 K). For the localized motion our results are consistent with H jumps within the hexagons formed by interstitial [Hf_2Cr_2] sites. It should be noted, however, that since there are two types of hexagons formed by these sites and the sites in type II hexagons are not equidistant, the detailed microscopic picture of H motion in C14-type compounds may imply more than two frequency scales.

The analysis of our proton spin-lattice relaxation data for $HfCr_2H_x$ ($0.30 \leqslant x \leqslant 1.62$) has shown that the electronic (Korringa) contribution to the relaxation rate, R_{1e}, increases significantly with increasing H content. Such a behaviour suggests that the density of electron states at the Fermi level in $HfCr_2H_x$ increases with increasing x. The motional (dipolar) contribution to the relaxation rate, $R_{1d}(T)$, exhibits a characteristic peak near 200 K; this peak is shown to originate from the slower H jump process. The hydrogen jump rate τ_d^{-1} in the region

of the peak is found to decrease with increasing H content, while the corresponding activation energy for H diffusion grows from 138 meV for $HfCr_2H_{0.30}$ to 177 meV for $HfCr_2H_{1.62}$.

Acknowledgments

The authors are grateful to J Combet for assistance with the QENS measurements at ILL and to D S Sibirtsev for assistance with the NMR measurements. This work was supported by the Russian Foundation for Basic Research (Grant No 03-02-16063), the Priority Programme 'Hydrogen Energy' of the Russian Academy of Sciences and the NATO Linkage Grant No HTECH.LG 973890.

References

[1] Skripov A V 2003 *Defect Diffus. Forum* **224/225** 75
[2] Skripov A V, Cook J C, Sibirtsev D S, Karmonik C and Hempelmann R 1998 *J. Phys.: Condens. Matter* **10** 1787
[3] Skripov A V, Cook J C, Udovic T J and Kozhanov V N 2000 *Phys. Rev.* B **62** 14099
[4] Bull D J, Broom D P and Ross D K 2003 *Chem. Phys.* **292** 153
[5] Hempelmann R, Richter D and Heidemann A 1982 *J. Less-Common Met.* **88** 343
[6] Bowman R C, Craft B D, Attalla A and Johnson J R 1983 *Int. J. Hydrogen Energy* **8** 801
[7] Morimoto K, Saga M, Fujii H, Okamoto T and Hihara T 1988 *J. Phys. Soc. Japan* **57** 647
[8] Skripov A V, Belyaev M Yu and Stepanov A P 1991 *Solid State Commun.* **78** 909
[9] Renz W, Majer G, Skripov A V and Seeger A 1994 *J. Phys.: Condens. Matter* **6** 6367
[10] Skripov A V, Pionke M, Randl O and Hempelmann R 1999 *J. Phys.: Condens. Matter* **11** 1489
[11] Sokolova E I, Padurets L N and Shilov A L 1988 *Zh. Neorg. Khim.* **33** 275
[12] Somenkov V A and Irodova A V 1984 *J. Less-Common Met.* **101** 481
[13] Kohlmann H, Fauth F, Fischer P, Skripov A V, Kozhanov V N and Yvon K 2001 *J. Alloys Compounds* **327** L4
[14] Skripov A V, Udovic T J and Huang Q 2005 at press
[15] Bée M 1988 *Quasielastic Neutron Scattering* (Bristol: Hilger)
[16] Hempelmann R 2000 *Quasielastic Neutron Scattering and Solid State Diffusion* (Oxford: Clarendon)
[17] Chudley C T and Elliott R J 1961 *Proc. Phys. Soc. (London)* **77** 353
[18] Havill R L, Titman J M, Wright M S and Crouch M A 1989 *Z. Phys. Chem. N. F.* **164** 1083
[19] Campbell S I, Kemali M, Ross D K, Bull D J, Fernandez J F and Johnson M R 1999 *J. Alloys Compounds* **293–295** 351
[20] Yvon K and Fischer P 1988 *Hydrogen in Intermetallic Compounds* vol I, ed L Schlapbach (Berlin: Springer) p 87
[21] Didisheim J J, Yvon K, Shaltiel D and Fischer P 1979 *Solid State Commun.* **31** 47
[22] Schönfeld C, Hempelmann R, Richter D, Springer T, Dianoux A J, Rush J J, Udovic T J and Bennington S M 1994 *Phys. Rev.* B **50** 853
[23] Cotts R M 1978 *Hydrogen in Metals* vol I, ed G Alefeld and J Völkl (Berlin: Springer) p 227
[24] Galoshina E V, Kozhanov V N and Skripov A V 2002 *Phys. Met. Metallogr.* **93** 48
[25] Bowman R C, Lynch J F and Johnson J R 1982 *Mater. Lett.* **1** 122
[26] Skripov A V and Belyaev M Yu 1993 *J. Phys.: Condens. Matter* **5** 4767
[27] Göring R, Lukas R and Bohmhammel K 1981 *J. Phys. C: Solid State Phys.* **14** 5675
[28] Bloembergen N, Purcell E M and Pound R M 1948 *Phys. Rev.* **73** 679
[29] Skripov A V, Rychkova S V, Belyaev M Yu and Stepanov A P 1990 *J. Phys.: Condens. Matter* **2** 7195
[30] Skripov A V, Soloninin A V, Stepanov A P and Kozhanov V N 1999 *J. Phys.: Condens. Matter* **11** 10393
[31] Stoddard R D and Conradi M S 1998 *Phys. Rev.* B **57** 10455
[32] Shinar J, Davidov D and Shaltiel D 1984 *Phys. Rev.* B **30** 6331
[33] Skripov A V, Belyaev M Yu, Rychkova S V and Stepanov A P 1991 *J. Phys.: Condens. Matter* **3** 6277
[34] Skripov A V, Cook J C, Karmonik C and Kozhanov V N 1999 *Phys. Rev.* B **60** 7238
[35] Sholl C A 1988 *J. Phys. C: Solid State Phys.* **21** 319